Coupling of Resonant Modes in Micromechanical Vibratory Rate Gyroscopes

A. S. Phani†, A. A. Seshia†, M. Palaniapan*, R. T. Howe ‡, J. Yasaitis**

† Department of Engineering, University of Cambridge, Cambridge, CB2 1PZ, UK
* Department of ECE, National University of Singapore, Singapore 117576
‡ Department of EECS, University of California, Berkeley, CA 94720, USA
** Analog Devices Inc., Cambridge, MA 02139, USA
E-mail: **aas41@eng.cam.ac.uk**

ABSTRACT

Analytical models are presented to describe the resonant modal coupling behaviour of z-axis micromechanical vibratory rate gyroscopes fabricated in an integrated polysilicon surface micromachining process. The models are then applied to predict the extent of displacement and force coupling between the drive and sense axes of this device as a function of varying degrees of matching between the resonant frequencies associated with these modes. Two modelling approaches are presented. The first approach is based on linear vibration analysis. The second approach− a state-space based system identification method− is used to calculate the anisoelasticity parameters. It is shown that, as the resonant frequencies of the two modes are brought closer together, an improvement in overall resolution and scale factor of the device is obtained at the expense of an enhanced coupling of forces to displacements between the two axes and the onset of electrostatic instability for an open-loop sensing implementation.

Keywords: micromechanical gyroscope, resonant coupling, surface micromachining.

1 Introduction

Vibratory microgyroscopes operate on the principle of resonant modal coupling through the Coriolis force. A typical single-axis resonant microgyroscope consists minimally of two degrees of freedom, such as two masses coupled by springs. The first mass, called the drive mass, is set to resonance by driving it at its natural frequency using lateral comb drive mechanisms. When the coupled system is placed on a rotating platform, the Coriolis force induces displacements in the second mass, called the sense mass. This motion is detected using capacitive sensing structures (see figure 1), allowing estimation of the angular motion of the platform. The coupling of motions of the two masses is not only due to the Coriolis force but also due to the elastic forces (through the off-diagonal stiffness terms) and the off-diagonal damping terms (arising due to non-proportional damping). This introduces errors in the measured displacements of the sense mass. While the off-diagonal stiffness terms give rise to quadrature errors *i.e.* errors in quadrature with the Coriolis component, the off-diagonal damping terms lead to in-phase errors. An approach to compensate for these errors is to design a control strategy to suppress the signals arising due to non-diagonal stiffness and damping terms [1] following the identification of these terms. The issue of identifying these matrices is discussed in a companion paper [2].

The focus of this paper is to develop analytical modelling techniques which can be used to predict the observed features in the sense output of a z-axis frame gyroscope described in [3]. Further details of the device are given in section 2. Experimental data, in the form of sense output spectrum, is presented and certain features of the data arising due to modal coupling are also described. Modelling of the device based on linear system theory and vibration analysis is described in section 3. A state-space based system identification approach is also presented to identify the angular mismatch between the drive-sense and principal stiffness axes. A comparison of the experimentally observed parameters, and those predicted by the modelling approach is given in section 4. Conclusions and further directions are summarised in section 5.

2 Device

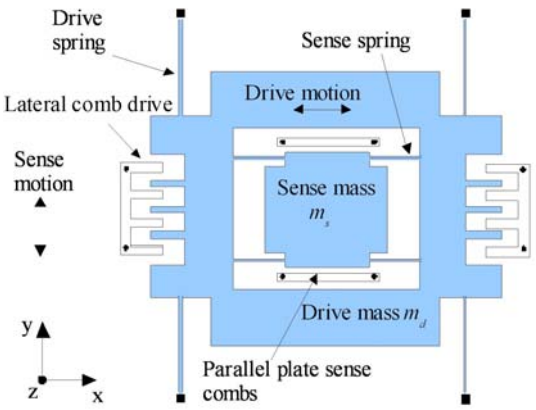

Figure 1: Schematic of a z-axis frame gyroscope with inner sensing and outer drive (ISOD) mechanism. See [3] for further details.

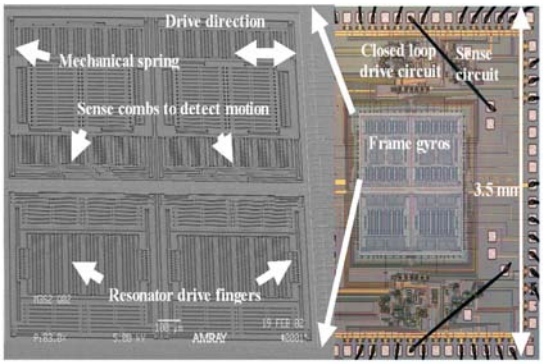

Figure 2: SEM and die photo of the frame microgyroscope fabricated in the Analog Devices Inc. Modular MEMS process.

A schematic of the device under consideration is shown in figure 1. It consists of two masses coupled via springs, the outer mass being attached to the substrate through a separate set of springs. The driven mode is excited by applying a force to the outer mass using an on-chip oscillator circuit and corresponds to the combined motion of the inner and outer mass along the x-axis. The sense mode corresponds to the case when the inner mass deflects relative to the outer mass along the y-axis. An SEM and chip micrograph of the gyroscope is shown in figure 2. The noise floor of the device is 0.01 deg/sec/$\sqrt{\text{Hz}}$. A detailed description of the gyroscope including rate data and functionality testing has been reported in [3].

2.1 Experiments

A limited set of experiments reveals the extent of modal coupling between the two axes. The driven mode is excited using an on-chip oscillator circuit described in [3]. A wideband electrostatic force input is applied to the inner mass along the y-axis using a separate set of electrodes. The sense mode frequency is tuned using a negative electrostatic spring effect and it is observed that the coupling from the force applied to the drive mass increases as a function of mode matching. The effect of mode matching under the described forcing conditions upon the output voltage spectrum of the gyroscope is shown in figure 3. It can be observed that the amplitude of the signal at the drive frequency increases when the sense mode is tuned to a frequency just below the drive resonance frequency. There is a characteristic anti-resonance behaviour at a frequency of about 16.327 kHz, where the output spectrum shows minimum response, both before and after the tuning of the sense mode. As the modes are brought closer together, the displacement of the structure along the sense direction increases due to the increased coupling between the two modes and a ceiling is reached governed by the electrostatic pull-in associated with the operation of the capacitive sensing structures [4].

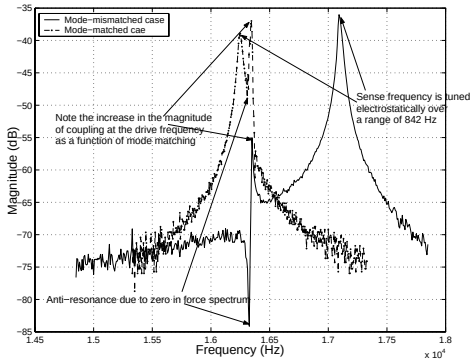

Figure 3: Experimentally observed output sense power spectrum corresponding to the displacement of the sense mass along the y-axis. Note the enhanced coupling of motion of the structure at the drive frequency when the modal frequencies are brought closer together. The measurements are made in the absence of an externally applied rotation rate.

3 Modelling

Two approaches to modelling the device dynamics are discussed in this section. The first approach is based on the frequency response analysis of linear vibrating systems. This technique can be used to predict the effect of modal coupling on the magnitude of the displacement of the inner mass along the y-axis as a function of mode matching. The second approach, based on state-space modelling, is used to identify the anisoelasticity parameters.

The governing equations of motion for a 2 DoF z-axis MEMS gyroscope can be written as:

$$\begin{bmatrix} m_d + m_s & 0 \\ 0 & m_s \end{bmatrix} \begin{bmatrix} \ddot{x} \\ \ddot{y} \end{bmatrix} + \begin{bmatrix} c_{dd} & c_{ds} \\ c_{sd} & c_{ss} \end{bmatrix} \begin{bmatrix} \dot{x} \\ \dot{y} \end{bmatrix} + \begin{bmatrix} k_{dd} & k_{ds} \\ k_{sd} & k_{ss} \end{bmatrix} \begin{bmatrix} x \\ y \end{bmatrix} = \begin{bmatrix} F_d \\ F_s \end{bmatrix} + \begin{bmatrix} 0 & 2m\Omega_z \\ -2m\Omega_z & 0 \end{bmatrix} \begin{bmatrix} \dot{x} \\ \dot{y} \end{bmatrix} + \begin{bmatrix} E_d \\ E_s \end{bmatrix} \quad (1)$$

where: m's, k's and c's are respectively the mass, stiffness and damping coefficients. Coriolis forces appear in the above equations of motion as $2m\Omega_z$ terms. F_d and F_s are the external forces applied to the gyroscope by the control system. The extraneous effects such as external accelerations, centrifugal force and z-axis motion feedthrough are lumped in the terms E_d and E_s. Subscripts d and s denote the the drive and sense directions of the gyroscope respectively. Note that, in the drive mode, the sense and drive masses move together and hence the corresponding mass term is $m_d + m_s$. A linear vibration analysis based modelling approach is described first.

3.1 Frequency Response Analysis

The equations of motion can be rewritten in the frequency domain in the form of an input-output relationship for the 2 DoF gyroscope as follows:

$$\{O\} = [H]\{F\} \tag{2}$$

where the output (displacement) vector $\{O\}$ and the input (force) vector $\{F\}$ are defined as:

$$\{O\} = \begin{bmatrix} O_d(\omega) \\ O_s(\omega) \end{bmatrix} \quad \{F\} = \begin{bmatrix} F_d(\omega) \\ F_s(\omega) \end{bmatrix} \tag{3}$$

and $[H]$ is the Frequency Response Function (FRF) matrix given by:

$$[H] = \begin{bmatrix} H_{dd}(\omega) & H_{ds}(\omega) \\ H_{sd}(\omega) & H_{ss}(\omega) \end{bmatrix}. \tag{4}$$

Using the equations of motion defined in equation 1 the expressions for the various FRFs can be written as:

$$H_{ss}(\omega) = \frac{D_{dd}(\omega)}{D_{ss}(\omega)D_{dd}(\omega) - (D_{sd}(\omega))^2} \tag{5}$$

$$H_{sd}(\omega) = -\frac{D_{sd}(\omega)}{D_{ss}(\omega)D_{dd}(\omega) - (D_{sd}(\omega))^2} \tag{6}$$

$$H_{dd}(\omega) = \frac{D_{ss}(\omega)}{D_{ss}(\omega)D_{dd}(\omega) - (D_{sd}(\omega))^2} \tag{7}$$

where

$$\begin{aligned} D_{dd}(\omega) &= k_{dd} - (m_d + m_s)\omega^2 + ic_{dd}\omega, \\ D_{ss}(\omega) &= k_{ss} - m_s\omega^2 + ic_{ss}\omega, \\ D_{sd}(\omega) &= k_{sd} + ic_{sd}\omega. \end{aligned} \tag{8}$$

Using equations 2, 3 and 4, the sense output of the gyroscope is given by:

$$O_s(\omega) = \underbrace{H_{ss}F_s(\omega)}_{\text{output due to force on the sense mass}} + \underbrace{H_{sd}F_d(\omega)}_{\text{output due to coupling}} \tag{9}$$

At the drive resonance frequency $\omega = \omega_d$, the term $H_{ss}(\omega_d)F_s(\omega_d)$ is much smaller compared to the other term in equation 9, since $H_{ss}(\omega)$ is a high-Q FRF with a peak at at ω_s. Hence, the sense output can be simplified as:

$$O_s(\omega_d) \approx H_{sd}(\omega_d)F_d(\omega_d). \tag{10}$$

Now the ratio of the sense output response under differing conditions of mode matching can be obtained as:

$$\frac{O_{s1}(\omega_d)}{O_{s2}(\omega_d)} \approx \frac{H_{sd1}(\omega_d)F_{d1}(\omega_d)}{H_{sd2}(\omega_d)F_{d2}(\omega_d)} \tag{11}$$

where the subscripts 1 and 2 refer to the two differing conditions of mode matching shown in figure 3. Substituting $H_{sd}(\omega)$ from equation 6, the ratio of sense outputs can be written as:

$$\frac{O_{s1}(\omega_d)}{O_{s2}(\omega_d)} = \frac{D_{dd2}(\omega_d)D_{ss2}(\omega_d) - (D_{sd2}(\omega_d))^2}{D_{dd1}(\omega_d)D_{ss1}(\omega_d) - (D_{sd1}(\omega_d))^2}. \tag{12}$$

Notice that the drive natural frequency (ω_d) remains unchanged before and after tuning as shown in figure 3. One can safely ignore terms like $(D_{sd}(\omega_d))^2$, provided the half power bandwidths of the two modes do not overlap, which is verified from the experimental data. With this simplification, the ratio of the sense outputs before and after tuning, using the definitions in equation 8, is given by:

$$\frac{O_{s1}(\omega_d)}{O_{s2}(\omega_d)} \approx \frac{c_{dd2}(k_{ss2} - m_s\omega^2 + ic_{ss2}\omega)}{c_{dd1}(k_{ss1} - m_s\omega^2 + ic_{ss1}\omega)}. \tag{13}$$

At the sense resonance frequency $\omega = \omega_s$, $F_d(\omega_s) \approxeq 0$ and hence the ratio of sense outputs at the sense resonance frequency, using equation 9, is given by:

$$\frac{O_{s1}(\omega_{s1})}{O_{s2}(\omega_{s2})} = \frac{H_{ss2}(\omega_{s2})F_{s2}(\omega_{s2})}{H_{ss1}(\omega_{s1})F_{s1}(\omega_{s1})}. \tag{14}$$

In this case also, the sense-sense FRF can be simplified, by ignoring terms containing $D_{sd}(\omega)$ as :

$$\begin{aligned} H_{ss}(\omega) &\approx \frac{D_{dd}(\omega)}{D_{dd}(\omega)D_{ss}(\omega)} \\ &= \frac{1}{D_{ss}(\omega)}. \end{aligned} \tag{15}$$

By using the definition of $H_{ss}(\omega)$ from equation 8 in the above equation, the ratio of the gyroscope output at the sense resonance frequencies before and after tuning is given by:

$$\frac{O_{s1}(\omega_{s1})}{O_{s2}(\omega_{s2})} \approx \frac{c_{ss2}\omega_{s2}}{c_{ss1}\omega_{s1}}. \tag{16}$$

By considering the magnitude of the cross FRF $H_{sd}(\omega)$ at the drive resonant frequency, and with the simplification described above, one obtains an approximate expression for the cross coupling stiffness as:

$$\begin{aligned} k_{sd} &\approx |H_{sd}(\omega_d)|c_{dd}\omega_d\sqrt{(k_{ss} - m_s\omega_d^2)^2 + \omega_d^2c_{ss}^2} \\ &= \left|\frac{O_s(\omega_d)}{F_d(\omega_d)}\right| c_{dd}\omega_d\sqrt{(k_{ss} - m_s\omega_d^2)^2 + \omega_d^2c_{ss}^2} \end{aligned} \tag{17}$$

Estimating k_{sd} by using the above equation requires an accurate estimation of the diagonal damping terms, especially c_{dd}. An alternate method of measuring k_{sd} is to measure the output of the device in presence of a known applied rotation rate. The output voltage spectrum of the device in response to a sinusoidal rotation rate at 7 Hz is shown in figure 7 of [3]. The magnitude of the sense output displacement at the drive resonant frequency now differentiates between the two terms in equation 9. The DC term corresponds to the coupling of modes due to anisoelasticity while the AC term corresponds to coupling due to the Coriolis force. A ratio of these two terms gives an estimate for k_{sd}. An equation for k_{sd} can now be written as:

$$k_{sd} \approx 2(m_s + m_d)\Omega\omega_d\frac{O_s}{O_{sc}} \tag{18}$$

Parameter	Theory	Experiment
Ratio of sense mode displacements before and after sense mode tuning at drive resonance frequency	0.121	0.126
Ratio of sense mode displacements before and after sense mode tuning at sense resonance frequencies	1.15	1.25
Instability point proof mass voltage (V)	9.9 V	9.6 V
Cross-coupling spring constant, k_{sd}		1.6×10^{-4} N/m

Table 1: Comparison of predicted and experimental parameters. Subscripts 1, 2 refer to mode-mismatched and mode-matched cases respectively. m, k, c and ω denote mass, stiffness, damping and resonant frequency.

where Ω is the applied rotation rate, O_s and O_{sc} are the sense outputs due to anisoelasticity (DC term) and applied rotation rate (AC term) respectively. An estimate for k_{sd} based on this analysis is shown in Table 1.

As the modes are tuned by varying the DC voltage on the proof mass, the sense displacement increases due to the increased coupling between the two modes and a ceiling is reached governed by electrostatic pull-in associated with the operation of the capacitive sensing structures. The expected point for the observation of electrostatic instability can be computed by following an analysis similar to that described in [4]. A good match is obtained between experiment and theory for the pull-in voltage as shown in Table 1. This instability limits the difference in the drive and sense frequencies.

3.2 State-Space Modelling

A state-space based modelling approach is used to identify the anisoelasticity parameters [2]. Figure 4 shows an 8th order model fitted to the measured sense output spectrum. This higher order model is reduced to a 4th order model (corresponding to the 2 physical modes of vibration) using the balanced reduction technique. The anisoelasticity *i.e.* the angular mismatch between the principal stiffness axes and the drive-sense directions is found to be 8^o under the mode mismatched conditions.

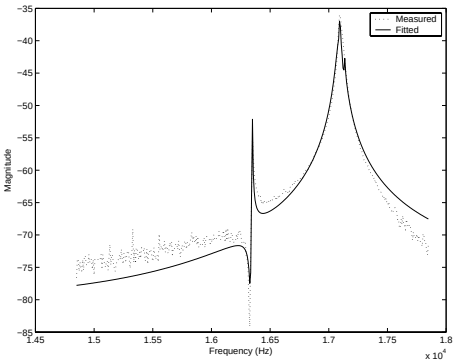

Figure 4: An 8th order fit to the measured output spectrum for the mode-mismatched case.

4 Comparison with experiment

The first row in Table 1 compares model and experiment for ratios of the displacement of the sense mass along the y-axis at the drive resonance frequency under two different conditions of mode matching. The second row in Table 1 compares model and experiment for ratios between the observed displacements of the inner mass along the y-axis at the sense resonance frequency under two different conditions of mode matching. The off-diagonal spring constant can be calculated as shown in equation 18. The predicted values for the ratios of displacements as a function of mode matching and the expected point for the observation of electrostatic instability are seen to closely match experiment.

5 Conclusion

Modal coupling in resonant z-axis frame gyroscopes has been investigated using the principles of linear vibration analysis and state-space modelling. These models are used to predict the features observed in the sense output spectrum of the device, as the drive and sense modal frequencies are brought closer through electrostatic tuning. Closed form expressions to predict the extent of observed modal coupling show a good match with experiments. A limit on the separation of the modal frequencies set by the electromechanical instability is also calculated and found to be in agreement with experiments. Future work will use these modelling principles for on-chip control algorithm implementation to suppress the errors due to modal coupling via off-diagonal stiffness and damping terms.

REFERENCES

[1] **Painter, C. C.** and **Shkel, A. M.**, SPIE Proceedings, March, 2001.

[2] **Phani, A. S.** and **Seshia, A. A.**, Nanotech 2004, 2004.

[3] **Palaniapan, M., Howe, R. T.** and **Yasaitis, J.**, IEEE-MEMS 2003, pp. 482–485, 2003.

[4] **Legtenberg, R., Groeneveld, A. W.** and **Elwenspoek, M.**, Journal of Micromechanics and Microengineering, Vol. 6, No. 3, pp. 320–329, 1996.